ORIGINAL ARTICLE

Fatigue behavior at flange thickness transitions with cope holes – design model for engineering practice

Christoph Derler[1]| Harald Unterweger[1]| Markus Knobloch[2]| Stefanie Röscher[2]

Correspondence

Christoph Derler
Graz University of Technology
Institute for Steel Structures
Lessingstraße 25
8010 Graz
Email: christoph.derler@tugraz.at

[1] Graz University of Technology, Austria

[2] Ruhr-University Bochum, Germany

Abstract

Flange thickness transitions are common constructional details in welded girders, such as crane runway girders or main girders of highway and railway bridges, to adapt the bending moment capacity of the girder to variable bending moment distributions. At these details the transverse butt weld is often decisive for the fatigue verification of the member. Based on comprehensive studies at Graz University of Technology, including also two fatigue tests, stress concentration factors for the fatigue verification of the butt welds at the girder flange were developed. However, due to the complex local stress fields at the flange thickness transition, cope holes were not included in these studies.

Within a research cooperation of Graz University of Technology and Ruhr University Bochum, flange thickness transitions with cope holes are studied recently. Based on comprehensive numerical FE- calculations within the practically relevant geometric parameter range, the complex local stress fields near the cope hole are analyzed both, within the web and the flange plate. For validation of the FE-model also strain measurements were carried out at large-scale test girders. Applying the hot spot stress method, the decisive hot spots are determined, and a simplified design model is developed for an accurate prediction of these hot spot stresses.

The paper presents this design model in detail and shows its accuracy - compared to the FE-results - for a wide range of different geometrical conditions, as used in practice (e.g. variation of girder dimensions, flange thickness ratio, tapering to the outside and to the inside).

Finally, also the results of full-scale fatigue tests on two different welded girders with flange thickness transitions and cope holes are presented. This provides an accurate fatigue resistance for the proposed design model, based on the hot spot stress method.

Keywords

Fatigue design, Structural Stress Method, Cope hole, Flange thickness transitions

1   Introduction

In the structural design of long span steel and composite girders, flange thickness transitions have always been a popular standard detail, to adjust the cross-sectional resistance to the variable bending moment distributions. Due to the sudden change in stiffness, these details cause additional local stresses, which need to be considered, especially for fatigue design. Based on extensive numerical investigations in [1-3], stress concentration factors for flanges with thickness transitions were developed, using the nominal stress approach. These rules are already included in the Austrian national annex to the current part 1-9 of Eurocode 3 (ÖN B 1993-1-9 [4]) and will also be introduced in the second generation of the Eurocodes, in

prEN 1993-1-9 [5]. However, these rules are not valid in combination with cope holes in the web (see Fig. 1), which
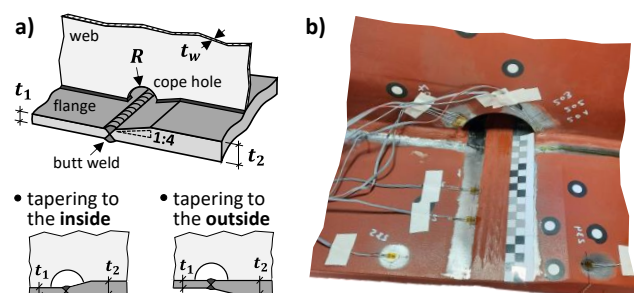

Figure 1 Flange thickness transition with a cope hole; a) schematic detail and different types of taper, b) execution in practice

is a very disadvantageous restriction for the assembly process, especially in steel bridge design.

To clarify the local fatigue behaviour of flange thickness transitions with an additional cope hole, this paper presents a comprehensive numerical investigation of the local stress fields. Two different types of execution – shown in Fig. 1a – are studied, the most common design with flange thickness tapering to the outside and also with thickness tapering to the inside (e.g. to facilitate the launching process for bridges). Based on the hot-spot stress method, a simplified design model for practice is proposed, to evaluate the decisive stress concentration factors (SCF) for fatigue assessment, at the beginning and the end of the cope hole (at the transition to the flange). A verification of the already derived SCFs for the flange butt weld at the thickness transition from [2], in combination with the cope hole can be found in [6].

In addition to the numerical investigations, also full-scale fatigue tests on different welded girders with flange thickness transitions and cope holes were performed. A comparison of the test results with suitable hot spot stress-based FAT classes proves the reliability of the proposed SCFs for fatigue verification.

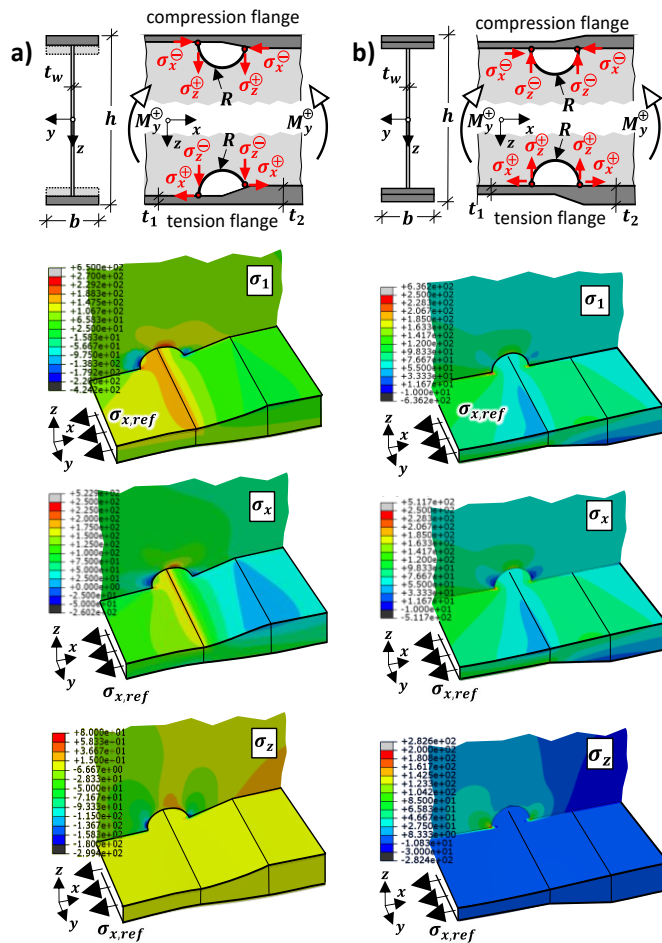## 2 Local load-carrying behaviour

2.1 Analysis of local stress fields

The combination of flange thickness transitions with a cope hole in the web results in a complex interaction of the associated local effects. For a basic understanding regarding the overall local behaviour of this detail, a numerical model of an I-shaped girder was developed, using practical dimensions and distinguishing both types of execution, flange thickness tapering to the inside (Fig. 2a) and also to the outside (Fig. 2b). The same finite element mesh was used, as later described in section 3.2. A cope hole radius of $R = 50$ mm and a flange thickness ratio of $t_1/t_2 = 40/80$ mm with a tapering ratio of 1:4 was considered. Pure bending load is assumed, with a nominal stress of $\sigma_{x,ref} = 100$ N/mm² at the thinner flange.

Fig. 2 shows the results of the numerical analysis, in terms of the local longitudinal and vertical stress fields σ_x and σ_z, as well as the principal stresses σ_1 in the vicinity of the cope hole at the tension flange. It should be noted that these are all structural stresses since the local weld geometry is consciously not included in the FE-model.

Beside the flange butt weld, especially at the beginning respectively end of the cope hole severe stress concentrations occur. At the latter points, the principal stresses σ_1 are oriented nearly vertical at the web plate (hence $\sigma_1 \approx \sigma_z$) and horizontally at the flange (hence $\sigma_1 \approx \sigma_x$). The direction of the local vertical stresses σ_z in the web depends on the direction of the flange thickness tapering. In case of flanges, tapering to the inside, vertical compressive stresses σ_z^- occur at the tension flange (see Fig. 2a). For flanges, tapering to the outside these are vertical tensile stresses σ_z^+ at the tension flange instead (see Fig. 2b).

For the chosen geometry in Fig. 2 ($t_1/t_2 = 40/80$ mm), the local stresses σ_x and σ_z for both types of execution (thickness tapering to the outside or inside) are in the same magnitude. However, σ_x is slightly higher in case of thickness tapering to the outside (approximately 30 %) and σ_z is instead slightly higher for flanges with tapering to the inside (approximately 15 %).

2.2 Critical positions and relevant stresses for fatigue verification

For fatigue design, beside the flange butt weld itself (see [4],[5] for details), the stress concentrations at the beginning and end of the cope hole must be considered. Therefore, the application of the structural hot-spot stress approach seems suitable. Two different hot-spots with associated locations of crack initiation respectively have to be distinguished (see Fig. 3).
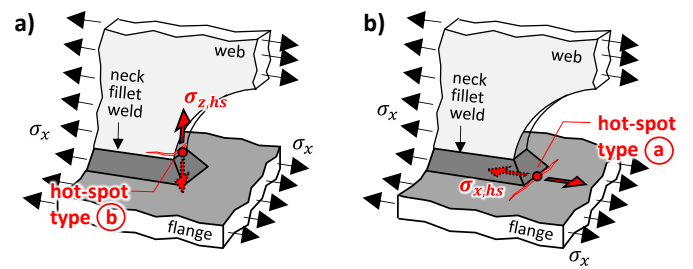

Figure 2 Local stress fields in the vicinity of the cope hole for a girder in pure bending M_y with $t_1/t_2 = 40/80\ mm$, $R = 50\ mm$, $b = 600\ mm$, $h = 3000mm$ and $\sigma_{x,ref} = 100\ N/mm^2$; a) flange thickness tapering to the inside, b) flange thickness tapering to the outside

Figure 3 Critical positions and relevant structural stresses for fatigue verification; a) vertical structural stress $\sigma_{z,hs}$ at the weld toe at the plate edge of the web, b) longitudinal structural stress $\sigma_{x,hs}$ at the weld toe at the flange plate

On the one hand, a fatigue crack may initiate from the weld toe of the neck fillet weld at the web plate, propagating into horizontal direction, perpendicular to the vertical stresses σ_z (see Fig. 3a). According to [7] this has to be classified as hot-spot type "b", indicating fatigue cracking at the plate edge of the web, with the relevant structural stress $\sigma_{z,hs}$.

On the other hand, a fatigue crack could also occur at the weld toe at the inner surface of the flange plate (see Fig. 3b), which propagates perpendicular to the local longitudinal stresses σ_x within the flange (see Fig. 3b). According to [7] this would be denoted as hot-spot type "a" instead.

3 Numerical parametric study

3.1 Scope of varied parameters

To investigate the influence of different girder and detail geometries on the magnitude of the relevant structural stresses $\sigma_{x,hs}$ and $\sigma_{z,hs}$, a comprehensive numerical study was carried out. The following essential geometry parameters were varied within a practical range:

- girder width (identical for both flanges):
  $b = 200; 400; 600; 800; 1000\ mm$
- girder height:
  $h = 1000; 2000; 3000; 4000; 5000\ mm$
- plate thickness of the thinner flange:
  $t_1 = 20; 40\ mm$
- flange thickness transition ratio:
  $t_2/t_1 = 1{,}1; 1{,}5; 2{,}5; 3{,}0$

The radius of the cope hole was kept constant with $R = 50\ mm$, the thickness of the web plate was assumed with $t_w = 10\ mm$ and the tapering ratio was chosen with 1:4 in all cases. The calculations were done for both types of flange thickness tapering, to the outside and to the inside. Two cases were investigated respectively, thickness tapering only at one flange (common for composite girders) or at both flanges.

Altogether over 150 FE calculations were done, providing also sufficient data for the proposal of a simplified design model for prediction of the structural stresses $\sigma_{x,hs}$ and $\sigma_{z,hs}$, which will be presented in section 4. An extract from the FE-results – already compared to the results of the proposed design formulae – is presented in Tab. 3.

Additional, individual calculations were also done for girders with higher flange plate thickness, up to $t_1 = 100\ mm$.

3.2 FE-model

All numerical calculations were executed with the software package of Abaqus. Fig. 4 illustrates the FE-model and its discretization of element sizes.

To save computational effort, the numerical model includes only a segment of the girder with the length L^* equal to the girder height. Within this length, all local stresses from the cope hole have completely subsided. Fictitious supports were situated at both end cross sections, with

additional coupling constraints to ensure plane cross-sectional deformation. Pure bending load is assumed throughout the whole numerical study, introduced by the end moments M_{ref} which are respectively calibrated to cause a nominal bending stress $\sigma_{x,ref} = 100\ N/mm^2$ in the thinner flange.

Quadratic continuum FE-elements (C3D20R) were selected for the flange plate and quadratic shell elements (S8R) were used for the web plate. The mesh density was chosen in accordance with the recommendations for evaluation of structural stresses from IIW [7]. The element size of the quadratic shell elements in the vicinity of the cope hole was selected with 10x10mm, suitable for determination of $\sigma_{z,hs}$ (hot-spot type "b", see Fig. 3a). Three solid elements were chosen in flange thickness direction, as recommended in [8] for application of the through thickness stress linearization method for evaluation of the structural stresses $\sigma_{x,hs}$ (hot-spot type "a", see Fig. 3b).

All calculations were executed with linear elastic material behaviour according to standard steel properties ($E = 210.000\ N/mm^2, \nu = 0{,}3$).

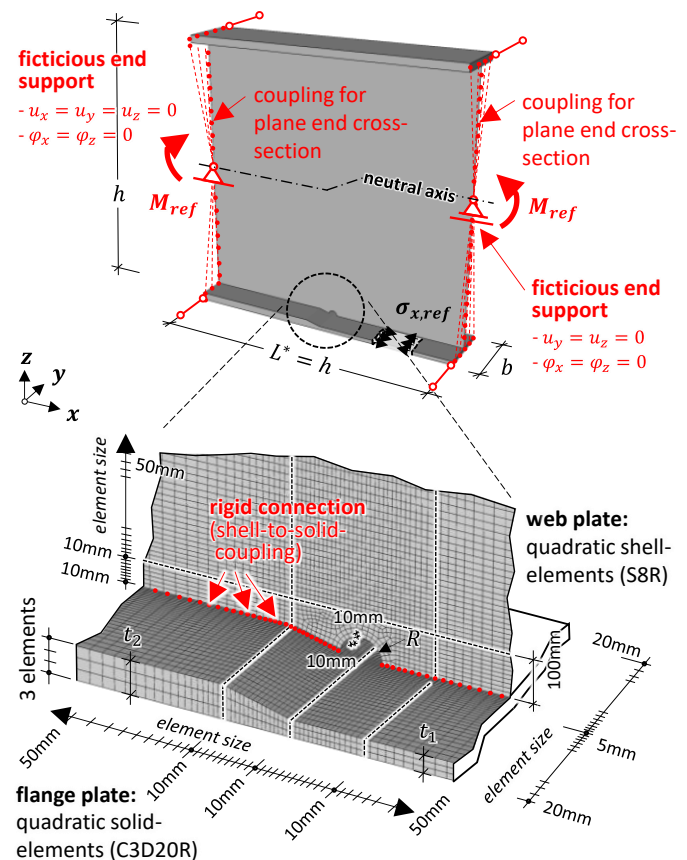**Figure 4** Finite element model for the numerical parametric study

3.3 Evaluation of the decisive structural stresses

This section describes the schematic procedure for evaluation of the critical hot-spot stresses $\sigma_{x,hs}$ and $\sigma_{z,hs}$ from the numerical computed local stress fields. Fig. 5 illustrates this procedure for a specific girder geometry, with flange thickness tapering to the inside ($t_1/t_2 = 40/80\ mm$) and a cope hole radius of R=50 mm.

The structural stress $\sigma_{z,hs}$ at the web plate (hot-spot type "b") is determined by the typical used surface extrapolation technique. Fig. 5a shows the stress distribution σ_1 and σ_z along the edge of the cope hole, with a continuous stress increase to the inner surface of the thicker flange. In the vicinity of the hot-spot, the vertical stresses σ_z are identical to the principal stresses σ_1. To comply with the rules of IIW [7] for the chosen mesh density of 10x10 mm, linear stress extrapolation was used, with the given extrapolation points at the edge of the cope hole, at a distance of 5 and 15 mm from the hot-spot (see Fig. 5a). The according extrapolation rule is given in Eq. 1.

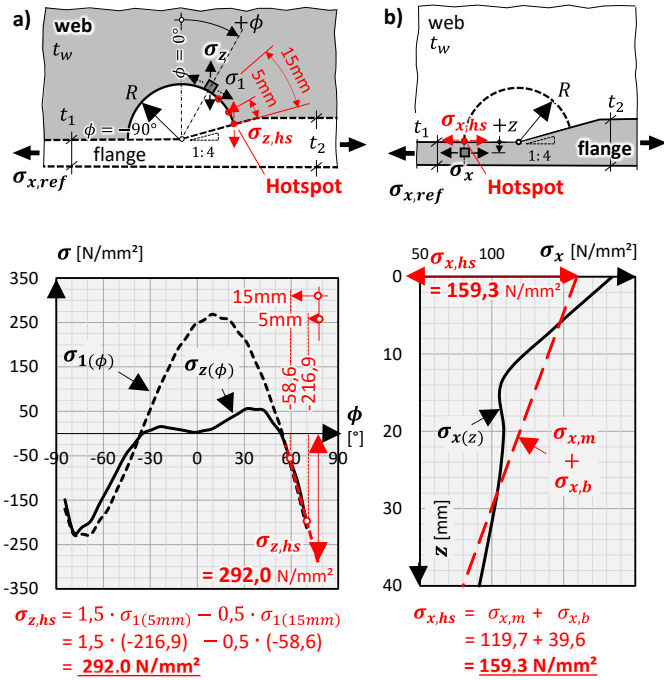$$\sigma_{z,hs} = 1{,}5 \cdot \sigma_{1(5mm)} - 0{,}5 \cdot \sigma_{1(15mm)} \tag{1}$$

Figure 5 Evaluation of the decisive structural stresses at the cope hole, for a girder in pure bending ($\sigma_{ref} = 100\ N/mm^2$) with $t_1/t_2 = 40/80\ mm$, $R = 50\ mm$, $b = 600\ mm$, $h = 3000\ mm$; a) $\sigma_{z,hs}$, b) $\sigma_{x,hs}$

For evaluation of the hot-spot stress $\sigma_{x,hs}$ (hot-spot type "a"), a stress extrapolation along the inner surface of the flange plate would lead to inappropriate results. Since the flange butt weld is close to the hot-spot at the end of the cope hole, the longitudinal stresses σ_x at the extrapolation points would also be affected by the stress concentration at the flange butt weld. This has also been pointed out in [9] and would lead to an underestimation of the hot spot stresses $\sigma_{x,hs}$. For this reason, an alternative approach was used, based on a linearization of the stresses σ_x through the thickness of the flange plate at the position of the hot-spot (see Fig. 5b). It was therefore necessary to integrate the stress distribution $\sigma_{x(z)}$, in order to obtain the the membrane stress $\sigma_{x,m}$ (see Eq. 2) and the bending stress $\sigma_{x,b}$ (see Eq. 3).

$$\sigma_{x,m} = \frac{1}{t_1} \cdot \int_0^{t_1} \sigma_{x(z)} \cdot dz \tag{2}$$

$$\sigma_{x,b} = \frac{6}{t_1^2} \cdot \int_0^{t_1} \sigma_{x(z)} \cdot \left(\frac{t_1}{2} - z\right) \cdot dz \tag{3}$$

Adding up both stress components, the structural hot-spot stress $\sigma_{x,hs}$ can then be written as:

$$\sigma_{x,hs} = \sigma_{x,m} + \sigma_{x,b} \tag{4}$$

3.4 Validation of the FE-results by experimental tests

In order to validate the numerical model for evaluation of the structural stresses at the cope hole, also local strain measurements have been carried out during static loading tests on two full-scale welded girders, which were finally also used for fatigue tests (see section 5). Fig. 6a shows the geometry of these test girders, with two symmetrically arranged flange thickness transitions ($t_1/t_2 = 20/40\ mm$) including a cope hole ($R = 50\ mm$), both at the upper- and lower flange. The only difference between the two girders is the execution of the neck weld in the vicinity of the cope hole. Girder G1 has neck fillet welds with $a_w = 5\ mm$, girder G2 has a fully penetrated butt weld. The test setup was chosen as a four-point bending test, to provide a constant bending moment between the two transverse stiffeners.

Fig. 6b shows the applied strain gauges (sg), along the edge of the cope holes. At the end of the cope holes at the thicker flange, three linear strain gauges were situated on both surfaces of the web respectively (S1-S3 and S1'-S3') at a distance of 5, 15 and 25mm to the weld toe of the neck fillet weld.
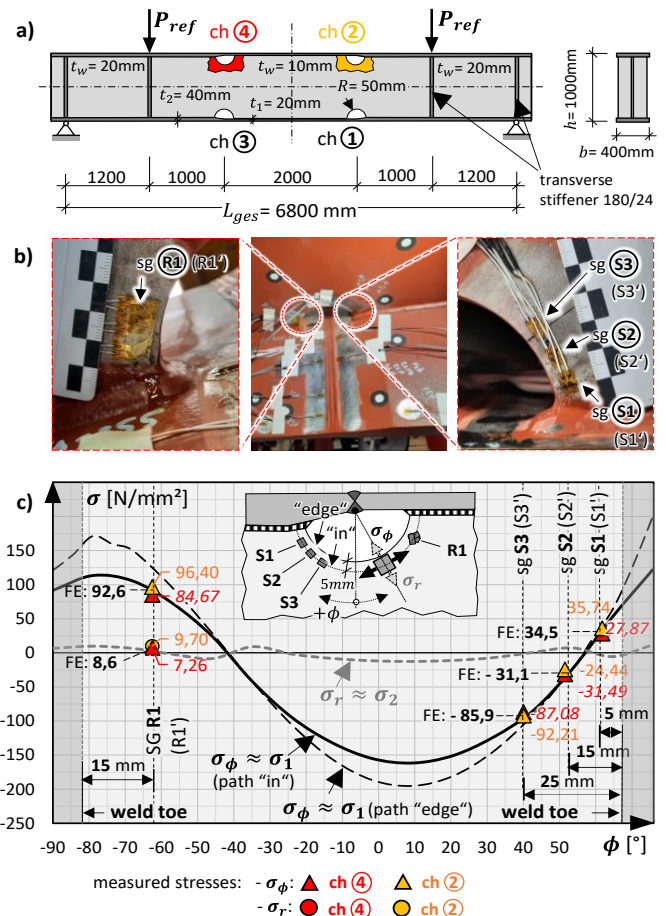

Figure 6 Static loading tests on a large-scale girder; a) geometry of the test girder, b) applied strain gauges at the cope holes, c) comparison between the FE-results and the strain gauge measurements for the local stresses around the cope hole

The measuring grid is oriented in tangential direction to the plate edge, so that the measured strains ε_ϕ correspond quite accurately to the principal strains ε_1. In perpendicular direction, radial to the free plate edge, the stresses σ_r are neglectable small (see also Fig. 6c), which allows direct evaluation of σ_1, using the one-dimensional Hooke's law $\sigma_1 = E \cdot \varepsilon_1$.

On the opposite end of the cope hole, near the thinner flange, additional strain gauge rosettes (R1 and R1' at the same position on both surfaces of the web) were applied, 15mm above the weld toe of the neck weld.

Fig. 6c shows a comparison between the numerically calculated stress distributions $\sigma_\phi \approx \sigma_1$ and $\sigma_r \approx \sigma_2$ along the edge of the cope hole and the results based on the strain measurements, both given for a nominal stress of $\sigma_{x,1} = 100\,N/mm^2$ at the thinner flange. The measurement results are related to test girder G1, with the neck fillet welds. However, similar results were obtained for test girder G2 with the full penetration welds. The yellow data points show the strain gauge results at detail ch2 and the red data points at detail ch4, both located at the compression flange of the girder (see Fig. 6a). These data points represent the mean value of the measured stresses on both surfaces of the web respectively. Since the axes of the strain gauges are not directly located at the edge of the cope hole, but 5mm further inside, Fig. 6c contains the numerical stress distributions for two result paths. In addition to the stresses $\sigma_\phi \approx \sigma_1$ along the cope hole edge (path "edge") also the stresses $\sigma_\phi \approx \sigma_1$ and $\sigma_r \approx \sigma_2$ along the inner path "in", passing through the positions of the strain gauges, are shown. The latter result curves must be considered when comparing the numerical calculations with the measurements.

For both details (ch2 and ch4), the measurement results show a good agreement with the numerical analysis, which means the structural FE-model is quite suitable for prediction of the hot-spot stresses.

4 Proposed design model for the relevant structural stresses

Based on the extensive numerical investigations, presented in section 3, and regression analysis of the results, a simplified design model could be proposed for estimation of the decisive structural stresses at the end of the cope hole. The according equations are given in section 4.1 and 4.2 and can directly be used for fatigue verification in combination with the structural hot-spot stress method.

4.1 Design model for the horizontal structural stress $\sigma_{x,hs}$ at the flange plate
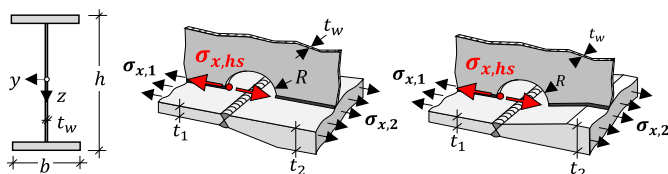

Figure 7 Structural stress $\sigma_{x,hs}$ at the weld toe at the flange plate

The proposed solution for the structural stress $\sigma_{x,hs}$ at the weld toe at the flange plate (see Fig. 7) is based on the stress concentration factor $k_{f,x}$ and the nominal longitudinal stress $\sigma_{x,1}$ due to global bending in the thinner flange. It can be written as:

$$\sigma_{x,hs} = k_{f,x} \cdot \sigma_{x,1} \tag{5}$$

For both types of execution (tapering to the inside or outside), the decisive hot-spot is always located at the thinner flange, as highlighted in Fig. 7. The stress concentration factor $k_{f,x}$ takes account for the interaction of both local effects, the stress increase due to the cope hole as well as the additional effect due to the flange thickness transition and the associated eccentricity of the flange normal forces.

- For flanges with thickness tapering to the inside, the estimation of $k_{f,x}$ is given as:

$$k_{f,x} = k_{f,x}^{(ch)} \cdot \left[1 - \lambda \cdot \left(\frac{t_2}{t_1} - 1 \right) \right] \tag{6}$$

- with: $\lambda = 0{,}4 - \dfrac{4\,t_1}{b} + \dfrac{0{,}2\,h}{5000}$ (7)

- For flanges with thickness tapering to the outside, $k_{f,x}$ can be estimated with:

$$k_{f,x} = k_{f,x}^{(ch)} \cdot \left[1 + \lambda \cdot \left(\frac{t_2}{t_1} - 1 \right) \right] \tag{8}$$

- with: $\lambda = 1{,}0 - \dfrac{16\,t_1}{b} + \dfrac{0{,}5\,h}{5000}$ (9)

where t_1 and t_2 are the plate thicknesses of the thinner respectively thicker flange plate, h is the girder height and b is the girder width (all values in mm).

In Eq. 6 and 8, the SCF $k_{f,x}^{(ch)}$ describes the stress increase due to the cope hole only, without additional thickness tapering of the flange plate. A suitable approximate solution therefore could be derived by additional numerical investigations with $t_1 = t_2$ (for lack of space not presented in this paper) and is summed up in Tab. 1.

Table 1 Stress concentration factor $k_{f,x}^{(ch)}$

$$k_{f,x}^{(ch)} = \frac{\sigma_{x,hs}^{(ch)}}{\sigma_x} = 1{,}65 \cdot \left(\frac{t_w}{t_f} \right)^{0{,}22} \cdot \left(\frac{R}{t_w} \right)^{0{,}15} \tag{10}$$

- for flanges tapered in thickness:
$$t_f = t_1$$

Eq. 10 contains two additional geometric parameters, the web plate thickness t_w and the cope hole radius R. For calculation of the overall SCF $k_{f,x}$ in case of flanges with additional thickness tapering at the cope hole (see Eq. 6 or 8), $k_{f,x}^{(ch)}$ has to be evaluated by replacing t_f with the plate thickness t_1 of the thinner flange.

As can directly be seen from the equations for the overall stress concentration factor $k_{f,x}$ (Eq. 6 and 8), for flanges with thickness tapering to the inside, the eccentricity of the flange normal forces has a beneficial effect on the

structural stress $\sigma_{x,hs}$, i.e. $k_{f,x} < k_{f,x}^{(ch)}$. However, for thickness transitions to the outside, the structural stress $\sigma_{x,hs}$ increases, i.e. $k_{f,x} > k_{f,x}^{(ch)}$ (see also Tab. 4).

4.2 Design model for the vertical structural stress $\sigma_{z,hs}$ at the web plate

The vertical structural stress $\sigma_{z,hs}$ at the weld toe at the web plate (see Fig. 8) can be estimated in the same manner as described for $\sigma_{x,hs}$ in section 4.1 before. Based on the nominal bending stress $\sigma_{x,1}$ at the thinner flange and the corresponding stress concentration factor $k_{f,z}$, the proposed solution for $\sigma_{z,hs}$ is given as:
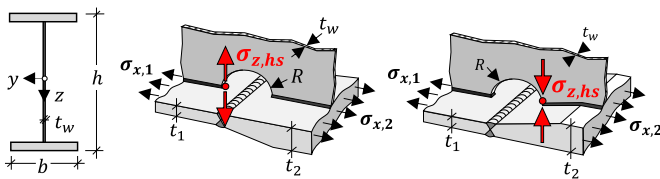
$$\sigma_{z,hs} = k_{f,z} \cdot \sigma_{x,1} \tag{11}$$

Figure 8 Structural stress $\sigma_{z,hs}$ at the weld toe at the web plate

This structural stress $\sigma_{z,hs}$, can directly be taken as the principal stress for fatigue verification of the web plate.

As shown in Fig. 8, the location of the decisive hot-spot depends on the direction of the flange thickness transition. For thickness tapering to the outside, the higher structural stress $\sigma_{z,hs}$ is expected at the cope hole end at the thinner flange (tension). In contrast, for flanges with thickness tapering to the inside, the higher structural stress $\sigma_{z,hs}$ occurs at the cope hole end at the thicker flange (compression).

The proposed solution for the stress intensity factor $k_{f,z}$ is obtained in Eq. 12 and 13.

- For flanges with thickness tapering to the inside:

$$k_{f,z} = k_{f,z}^{(ch)} + 3,8 \cdot k_{f,z}^{(tt)1,2} \tag{12}$$

- For flanges with thickness tapering to the outside:

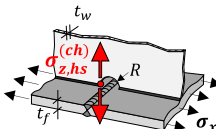$$k_{f,z} = k_{f,z}^{(ch)} + 3,8 \cdot k_{f,z}^{(tt)2,0} \tag{13}$$

These equations combine again both local effects, the vertical stress concentration in the web plate due to the cope hole and the additional stress increase due to the flange thickness transition. The former effect is represented by the component $k_{f,z}^{(ch)}$, the latter one is considered by $k_{f,z}^{(tt)}$.

The proposed expressions for both components $k_{f,z}^{(ch)}$ and $k_{f,z}^{(tt)}$ of the overall SCF $k_{f,z}$ are summed up in Tab. 2. Thereby the stress concentration factor $k_{f,z}^{(ch)}$ (see Eq. 14), which describes the vertical structural stress for cope holes

without flange thickness transition, was derived by additional numerical calculations with $t_1 = t_2$ and subsequent regression analyses. For calculation of the SCF $k_{f,z}^{(ch)}$, in case of flanges with additional thickness tapering at the cope hole it should be noted that the flange thickness t_f must be replaced by the average flange plate thickness $(t_1 + t_2)/2$.
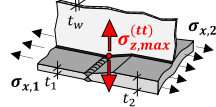
However, for the stress concentration factor $k_{f,z}^{(tt)}$ (see Eq. 15), which is defined by the ratio between the maximum vertical stress $\sigma_{z,max}^{(tt)}$ and the nominal bending stress $\sigma_{x,1}$ in case of flange thickness transitions without cope hole, a simplified design model was already suggested in [3]. This solution has been adopted and slightly modified for a better agreement with the FE-results.

Table 2 Stress concentration factors $k_{f,z}^{(ch)}$ and $k_{f,z}^{(tt)}$

$$k_{f,z}^{(ch)} = \frac{\sigma_{z,hs}^{(ch)}}{\sigma_x} = 0,92 \cdot \left(\frac{t_w}{t_f}\right)^{0,13} \cdot \left(\frac{t_w}{h_w}\right)^{0,09} \tag{14}$$

- for flanges tapered in thickness:
$$t_f = (t_1 + t_2)/2$$

$$k_{f,z}^{(tt)} = \frac{\sigma_{z,max}^{(tt)}}{\sigma_{x,1}} = \frac{2 \cdot V}{x_1 \cdot t_w \cdot \sigma_{x,1}} \tag{15}$$

-with:
- $M_{wb} = N_{fl,1} \cdot \frac{t_2 - t_1}{2} + \Delta N \cdot \frac{t_2}{2}$

- $V = \frac{M_{wb}}{e} = \frac{M_{wb}}{0,4 \cdot (x_1 + x_2)}$

- $x_1 = \alpha \cdot (t_1 \cdot f_b \cdot f_h)^{0,75};\ x_2 = \beta \cdot (t_2 \cdot f_b \cdot f_h)^{0,75}$
  - $\alpha = 26;\ \beta = 33$ ... for tapering to the inside
  - $\alpha = 23;\ \beta = 31$ ... for tapering to the outside

- $f_b = 1 + \frac{0,33}{400} \cdot (b\ [mm] - 600);\ f_h = \left(1 + \frac{0,6 \cdot h}{300 \cdot t_1}\right)^{1 - \frac{t_1}{t_2}}$

4.3 Accuracy of the proposed design model

The magnitude of the structural stresses $\sigma_{x,hs}$ and $\sigma_{z,hs}$ at the cope hole, for different girder geometries and different ratios of the flange thickness transition t_2/t_1 is presented in Tab. 3, each separately for thickness tapering to the inside and outside. In all cases, the radius of the cope hole is $R = 50\ mm$ and the nominal bending stress in the thinner flange is equal to $\sigma_{x,1} = 100\ N/mm^2$.

The table contains both, the exact results from the numerical FE-analysis (denoted as $\sigma_{x,hs,FE}$ and $\sigma_{z,hs,FE}$) as well as the estimated results based on the proposed design model from the previous sections 4.1 and 4.2 (denoted as $\sigma_{x,hs,model}$ and $\sigma_{z,hs,model}$). In addition, also the accuracy of these design equations is shown, indicated by the percentage deviations $\Delta\sigma_{x,hs}$ and $\Delta\sigma_{z,hs}$.

The achieved accuracy for both, the estimated structural stress $\sigma_{x,hs,model}$ with a maximum deviation of $\Delta\sigma_{z,hs} = 14,4\ \%$ and $\sigma_{z,hs,model}$ with $\Delta\sigma_{z,hs} = 9,4\ \%$ can be considered as sufficient for practise. In general, the results for flange tapering to the outside, show a slightly better accuracy.

Table 3 Structural stresses $\sigma_{x,hs}$ and $\sigma_{z,hs}$ for girders with lower flange thickness transition and cope hole; accuracy of proposed design model in comparison with FEM-analyses ($\sigma_{ref} = 100\ N/mm^2$)

#	t_1 [mm]	t_2 [mm]	t_2/t_1 [-]	h [mm]	b [mm]	$\sigma_{x,hs,FE}$ [N/mm²]	$\sigma_{x,hs,model}$ [N/mm²]	$\Delta\sigma_{x,hs}$ [%]	$\sigma_{z,hs,FE}$ [N/mm²]	$\sigma_{z,hs,model}$ [N/mm²]	$\Delta\sigma_{z,hs}$ [%]	$\sigma_{x,hs,FE}$ [N/mm²]	$\sigma_{x,hs,model}$ [N/mm²]	$\Delta\sigma_{x,hs}$ [%]	$\sigma_{z,hs,FE}$ [N/mm²]	$\sigma_{z,hs,model}$ [N/mm²]	$\Delta\sigma_{z,hs}$ [%]
						flange thickness tapering to the **inside**						flange thickness tapering to the **outside**					
				3000	200	**171,2**	178,9	+ 4,4	114,4	113,5	-0,8	**177,3**	189,3	+ 6,7	101,8	105,9	+ 4,1
	20	22		1000	400	**164,1**	177,4	+ 8,1	109,6	110,0	+0,3	**170,5**	185,7	+ 8,9	96,7	101,5	+ 5,0
				3000	400	**172,0**	178,9	+ 4,0	115,1	116,6	+1,2	**177,6**	189,3	+ 6,6	100,1	106,6	+ 6,5
1			1,1	5000	400	**173,0**	180,3	+ 4,3	118,2	119,6	+1,2	**179,7**	192,9	+ 7,3	101,1	109,0	+ 7,8
				1000	600	**148,2**	153,3	+ 3,5	105,4	106,4	+0,9	**143,4**	155,2	+ 8,2	87,0	93,9	+ 7,9
	40	44		3000	600	**154,9**	154,6	- 0,2	107,6	112,9	+5,0	**141,1**	158,3	+ 12,2	93,5	99,0	+ 5,9
				5000	600	**156,4**	155,8	- 0,4	108,3	116,4	+7,5	**143,2**	161,4	+ 12,7	95,8	101,5	+ 6,0
				3000	200	**172,8**	173,0	+ 0,1	158,3	152,3	-3,8	**238,4**	225,0	- 5,6	114,9	121,6	+ 5,8
	20	30		1000	400	**161,7**	165,7	+ 2,5	160,3	153,6	-4,2	**225,3**	206,9	- 8,1	109,8	120,1	+ 9,4
				3000	400	**172,2**	173,0	+ 0,4	170,4	167,7	-1,6	**245,3**	225,0	- 8,3	123,6	132,4	+ 7,1
2			1,5	5000	400	**174,8**	180,2	+ 3,1	173,4	172,2	-0,7	**253,5**	243,0	- 4,2	129,0	136,6	+ 5,9
				1000	600	152,1	147,3	- 3,1	**171,7**	175,5	+2,2	**149,8**	156,6	+ 4,5	136,1	132,2	- 2,8
	40	60		3000	600	166,4	153,5	- 7,7	**183,6**	189,8	+3,4	**165,0**	172,1	+ 4,3	157,8	149,6	- 5,2
				5000	600	168,8	159,7	- 5,4	**187,1**	198,2	+6,0	170,9	187,6	+ 9,8	**171,2**	159,0	- 7,1
				1000	200	144,8	151,1	+ 4,3	**166,5**	179,5	+7,8	**258,3**	233,4	- 9,7	144,1	138,2	- 4,1
				3000	200	166,9	165,5	- 0,8	**185,0**	198,8	+7,5	**292,0**	269,4	- 7,7	167,8	158,9	- 5,3
				1000	400	137,5	151,1	+ 9,9	**188,7**	202,9	+7,6	**272,5**	233,4	- 14,4	163,3	159,8	- 2,2
				2000	400	153,4	158,3	+ 3,2	**201,5**	217,1	+7,7	**292,9**	251,4	- 14,2	179,6	177,4	- 1,2
	20	40		3000	400	162,6	165,5	+ 1,7	**210,8**	224,4	+6,4	**305,4**	269,4	- 11,8	188,9	186,5	- 1,3
				4000	400	168,9	172,7	+ 2,2	**217,5**	227,8	+4,8	**314,1**	287,5	- 8,5	195,6	190,9	- 2,4
				5000	400	173,6	179,9	+ 3,7	**222,4**	229,0	+3,0	**321,0**	305,5	- 4,8	200,5	192,4	- 4,0
			2,0	1000	600	128,7	139,0	+ 8,0	**204,8**	211,1	+3,1	**283,7**	281,5	- 0,8	175,2	168,1	- 4,1
				1000	800	129,2	133,0	+ 2,9	**216,6**	213,3	-1,6	**293,2**	305,5	+ 4,2	184,3	170,3	- 7,6
				3000	800	142,3	147,4	+ 3,6	**234,0**	227,9	-2,6	**321,6**	341,6	+ 6,2	208,2	190,6	- 8,4
3				1000	600	142,3	139,6	- 1,8	**265,0**	254,1	-4,1	173,7	158,1	- 8,9	**216,0**	210,1	- 2,7
				2000	600	152,5	145,8	- 4,4	**279,6**	264,8	-5,3	186,6	173,6	- 6,9	**236,7**	234,8	- 0,8
	40	80		3000	600	159,3	152,0	- 4,6	**292,0**	274,0	-6,2	194,0	189,1	- 2,5	**248,9**	251,2	+ 0,9
				4000	600	164,5	158,2	- 3,8	**301,3**	281,0	-6,7	199,2	204,6	+ 2,7	**257,6**	263,3	+ 2,2
				5000	600	168,7	164,4	- 2,6	**308,7**	286,2	-7,3	203,3	220,1	+ 8,2	**264,4**	272,2	+ 3,0

5 Fatigue tests

5.1 Scope and test procedure

Finally, also full-scale fatigue tests were conducted, using the same two test girders (steel grade S355) and the same four-point bending condition as for the static load tests, already discussed and shown in Fig. 6a. Both test girders have the same geometry, however, as already mentioned before, test girder G1 is executed with neck fillet welds of $a_w = 5$ mm and girder G2 has full penetration butt welds in the vicinity of the cope hole. Each test girder contains four identically designed cope hole details with $R = 50$ mm and an additional thickness transition of the flange plate $t_1/t_2 = 20/40$ mm with a tapering ratio of 1:4 (see also Fig. 6a).

The load range of the constant amplitude loading ΔP was set to be 711 kN, with a load ratio $P_{min}/P_{max} = 0,1$. Hence the nominal stress range in the thinner flange was equal to $\Delta\sigma_{x,1} = 175\ N/mm^2$ at all four cope hole details. The according local structural stress ranges at the end of the cope holes, obtained by the proposed design equations, are $\Delta\sigma_{x,hs} = k_{f,x} \cdot \Delta\sigma_{x,1} = 1,51 \cdot 175 = 264,3\ N/mm^2$ and $\Delta\sigma_{z,hs} = k_{f,z} \cdot \Delta\sigma_{x,1} = 2,02 \cdot 175 = 353,5\ N/mm^2$.

The test procedure is shown in Fig. 9a and consisted of two steps respectively. In the first step, the fatigue load was applied until fatigue cracking occurred at the flange butt weld at the lower flange (details ch1 and ch3). This happened at both girders G1 and G2. These details were then reinforced by bolted splice plates and in a second step, the fatigue tests were continued in reversed girder position, with the cope hole details ch2 and ch4, originally located at the compression flange, now situated at the tension flange (see Fig. 9a).

Table 4 Number of applied load cycles N during the fatigue tests

girder	detail	test step	number of load cycles	
			hot-spot "a" ($\sigma_{x,hs}$)	hot-spot "b" ($\sigma_{z,hs}$)
G1	ch1 & ch3	1	480.000 ($\Delta\sigma^+$)	480.000 ($\Delta\sigma^-$)
		2	- (reinforced)	
		N_{tot} [N^*_{tot}]	**480.000**	**480.000** [103.680*]
	ch2 & ch4	1	480.000 ($\Delta\sigma^-$)	480.000 ($\Delta\sigma^+$)
		2	350.000 ($\Delta\sigma^+$)	350.000 ($\Delta\sigma^-$)
		N_{tot} [N^*_{tot}]	**830.000** [453.680*]	**830.000** [555.600*]
G2	ch1 & ch3	1	278.500 ($\Delta\sigma^+$)	278.500 ($\Delta\sigma^-$)
		2	- (reinforced)	
		N_{tot} [N^*_{tot}]	**278.500**	**278.500** [60.156*]
	ch2 & ch4	1	278.500 ($\Delta\sigma^-$)	278.500 ($\Delta\sigma^+$)
		2	263.000 ($\Delta\sigma^+$)	263.000 ($\Delta\sigma^-$)
		N_{tot} [N^*_{tot}]	**541.500** [323.156*]	**830.000** [335.308*]

Hence, also the direction of the local stresses $\sigma_{x,hs}$ change from compressive cycles $\Delta\sigma^-$ to tensile cycles $\Delta\sigma^+$ and vice versa the local stresses $\sigma_{z,hs}$ change from tensile to compressive direction. The number of applied load cycles N

during the individual test steps 1 and 2 are summarized in Tab. 4, with the according direction of the local stress cycles (tensile $\Delta\sigma^+$ or compressive $\Delta\sigma^-$) for both observed hot spots, type "a" and type "b" respectively.

5.2 Results

In case of both tested girders, G1 and G2, at all 2x4=8 observed cope hole details, fatigue cracking always occurred at the weld toe of the flange butt weld at the thickness transition only. No cracks were detected at the end of the cope holes, neither due to the vertical stresses $\sigma_{z,hs}$ at the web plate, nor due to the longitudinal stresses $\sigma_{x,hs}$ at the flange plate. Hence, all evaluated fatigue test data for both hotspots at the cope hole end, type "a" with $\sigma_{z,hs}$ (shown in Fig. 9b) and type "b" with $\sigma_{x,hs}$ (shown in Fig. 9c), have to be considered as runouts.
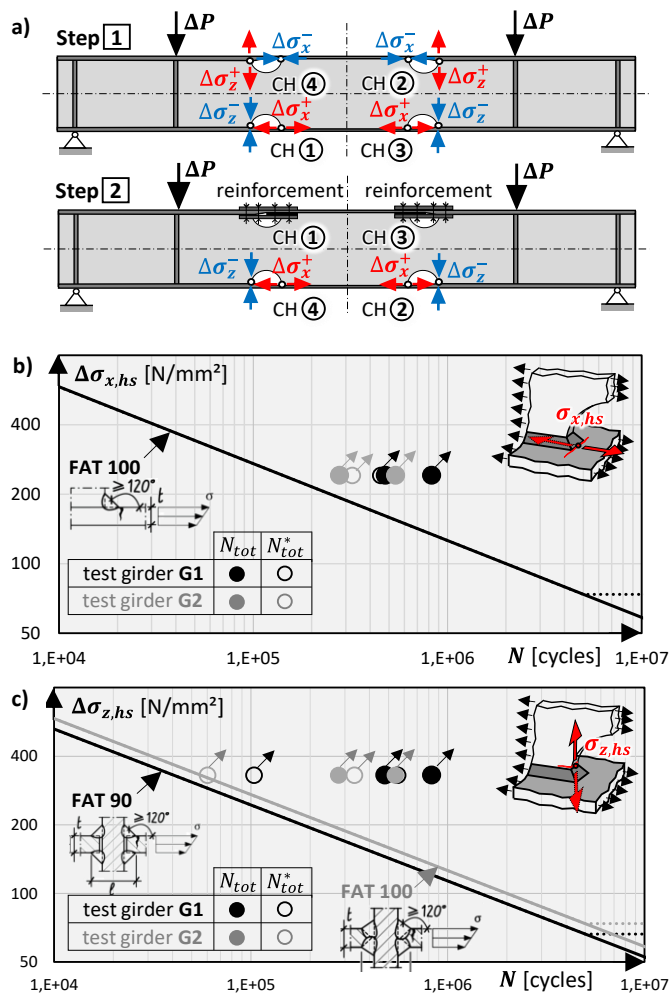

Figure 9 Full-scale fatigue tests; a) test girder and test procedure, b) evaluation of the fatigue tests for (equivalent) structural stresses $\sigma_{x,hs}$, c) evaluation of the fatigue tests for (equivalent) structural stresses $\sigma_{z,hs}$

For both individual hotspots, the total number of applied load cycles (during test step 1 and 2) were calculated with two different approaches regarding the assessment of the compressive stress cycles $\Delta\sigma^-$. On the one hand, according to the provision of EN 1993-1-9 for welded details, the compressive cycles $\Delta\sigma^-$ are considered to have the same fatigue damage as the tensile stress cycles $\Delta\sigma^+$, due to the assumption of high tensile residual stresses in magnitude of the yield strength. In this case, the total number of load

cycles N_{tot} for the individual hot-spot is directly given by:

$$N_{tot} = N(\Delta\sigma^+) + N(\Delta\sigma^-) \qquad (12)$$

On the other hand, only if the residual stresses would be neglectable small, according to EN 1993-1-9, stress cycles in compression may be considered with an effective stress range of $0{,}6 \cdot \Delta\sigma^-$. This means, damage equivalently, the number of compressive stress cycles $N(\Delta\sigma^-)$ can be reduced by $0{,}6^m$, with m=3. In this case, the modified total number of load cycles N_{tot}^* for the individual hot-spot can be written as:

$$N_{tot}^* = N(\Delta\sigma^+) + 0{,}6^m \cdot N(\Delta\sigma^-) \qquad (12)$$

Both results, the total load cycles N_{tot} and N_{tot}^* are specified in Tab. 4, for each observed hot-spot respectively.

Finally, Fig. 9b and Fig. 9c show the fatigue test data of all 8 cope hole details, with the applied stress ranges $\Delta\sigma_{x,hs}$ and $\Delta\sigma_{z,hs}$, in relation to the total number of load cycles N_{tot} (respectively N_{tot}^*). For comparison also the fatigue resistance according to the applicable hotspot stress-based FAT classes from [5] are shown. This would be FAT 100 for the structural stresses $\Delta\sigma_{x,hs}$ at the flange plate (see Fig. 9b). For the structural stresses $\Delta\sigma_{z,hs}$, the appropriate FAT class depends on the execution of the neck weld, with FAT 90 for fillet welds (girder G1) and FAT 100 for full penetration welds (girder G2). In all cases, the fatigue test data are above the according S-N curve.

6 Conclusion and Outlook

This paper dealt with the fatigue behaviour of cope hole details with flange thickness transitions in welded steel or composite girders.

- The local stress fields at the cope hole were analysed, and the decisive hot-spot locations for fatigue verification were pointed-out.

- Based on an extensive parametric study, a simplified design model for the structural hot-spot stresses was developed, which can directly be used for fatigue verification in practise.

- The reliability of the proposed design model was verified by full-scale fatigue tests, indicating a higher fatigue resistance than the applicable hot-spot FAT classes from [5]

- Further fatigue tests will be performed on a third test girder in the near future, with an increased flange thickness transition of $t_1/t_2 = 20/50$ mm.

- Currently, also additional numerical calculations take place, investigating the influence of additional shear load.

7 Acknowledgements

References

[1] Greiner, R.; Taras, A.; Unterweger, H. 2009. „Tragverhalten an Gurtdickensprüngen geschweißter Biegeträger". Stahlbau 78, No.7, pp. 451–461

[2] Taras, A.; Unterweger, H. 2013. „Proposal for a stress modification factor for the fatigue design of flange thickness transitions in welded girders". Engineering Structures 56, pp. 1758–1774

[3] Unterweger, H.; Taras, A.; Puig, M. G. 2014. „Gurtdickensprünge geschweißter Biegeträger -Bemessungsbehelf für die komplexen lokalen Zusatzbeanspruchungen". Stahlbau 83, No.8, pp. 542–552

[4] ÖNORM B 1993-1-9:2017 NA:03/2017 Eurocode 3: Bemessung und Konstruktion von Stahlbauten - Teil 1-9: Ermüdung, Nationaler Anhang Österreich

[5] prEN 1993-1-9:12/2020. Eurocode 3: Design of steel structures-Part 1-9: Fatigue, Final Draft, CEN/TC250/SC3 N3268

[6] Röscher, S.; Knobloch M.; Derler, C.; Langwieser, M.; Unterweger, H. (2023), Fatigue behaviour of girder with flange thickness transitions and cope holes based on tests and numerical simulations, Submitted for Eurosteel 2023

[7] IIW-Documentation 1823-07: Recommendations for Fatigue Design of Welded Joints and Components, International Institute of Welding, 2008

[8] Poutiainen I.; Tanskanen P.; Marquis G.: Finite element methods for structural hot spot stress determination – a comparison of procedures, In: International Journal of Fatigue 26 (2004), pp. 1147-1157

[9] Röscher, S.; Knobloch, M. (2021), Fatigue Life Prediction of Welded Girders with Flange Thickness Transition and Cope Hole, in: Proceedings of Eurosteel 2021